CSIRO PUBLISHING

International Journal of Wildland Fire **2010**, *19*, 284–298 www.publish.csiro.au/journals/ijwf

Convective heat transfer in fire spread through fine fuel beds

W. R. Anderson[A], *E. A. Catchpole*[A] *and B. W. Butler*[B,C]

[A]University of New South Wales at ADFA, Canberra, ACT 2600, Australia.
[B]US Forest Service, Rocky Mountain Research Station, 5775 Hwy 10 W, Missoula, MT 59808, USA.
[C]Corresponding author. Email: bwbutler@fs.fed.us

Abstract. An extensive set of wind-tunnel fires was burned to investigate convective heat transfer ahead of a steadily progressing fire front moving across a porous fuel bed. The effects of fuel and environmental variables on the gas temperature profile and the 'surface wind speed' (gas velocity at the fuel bed surface) are reported. In non-zero winds, the temperature of the air near the fuel bed surface decays exponentially with distance from the fire front. In zero winds, the temperature decreases rapidly within a very short distance of the flame front, then decays slowly thereafter. The maximum air temperature decreases as the free stream wind speed, packing ratio and fuel moisture content increase. The characteristic distance of the exponential decay increases strongly with the free stream wind speed and decreases with the packing ratio and surface area-to-volume ratio of the fuel. The surface wind speed depends strongly on the free stream wind speed, and to a lesser extent on packing ratio, fuel bed depth and fuel moisture content. There are three general regimes for the surface flow: (1) a constant velocity flow of approximately half the free stream flow, far from the flame front; (2) an intermediate zone of minimum flow characterised by low or reversed flow; and (3) a region near the flame front where the velocity rises rapidly almost to the free stream velocity. The boundaries between the three regions move further from the flame front with increasing wind speed, in a way which is only slightly affected by fuel geometry.

Additional keywords: characteristic heating distance, kiel-static probe, radiation, thermocouple, wildland fire, wind tunnel.

Introduction

Most physical and semi-physical models for the steady rate of spread of a fire through a homogeneous fuel bed are based on an energy balance for a small volume element, comprised of fuel particles and air. They also generally assume that the fuel particles are randomly arranged and thermally thin so that each volume element has a well defined fuel temperature (Rothermel 1972; Pagni and Peterson 1973; Albini 1985; Clark 1996; Linn *et al*. 2003; Morvan and Dupuy 2004; Koo *et al*. 2005; Seron *et al*. 2005; Mell *et al*. 2006). In quasi-steady-state conditions, where the rate of spread is constant, the temperature of a volume element at the fuel surface then depends on its distance from the flame front.

The energy balance for a surface volume element equates the net effect of heat input and heat loss in a small interval of time with the corresponding increase in internal energy of the fuel element. The flame front is determined to have reached the fuel element when the temperature of the fuel element reaches a specified ignition temperature.

The rate of convective heat input per unit volume of fuel bed in the presence of gas at temperature T_g is:

$$\hbar s \beta (T_g - T) \quad (1)$$

(e.g. Raupach and Shaw 1982). Here, s is the particle surface area-to-volume ratio, β is the fuel bed packing ratio (the fraction of the fuel bed volume that is filled with solid fuel particles) and T is the fuel temperature (see *Glossary* for definitions of all variables used). The gas may range from a mixture of air and pyrolysis gases at flame temperature, moving at fairly high velocity and turbulent, to still air at ambient temperature (in which case (1) may become a cooling term). The average convective heat transfer coefficient $\hbar$ depends mainly on particle size and on the gas velocity. It is also weakly dependent on the particle and gas temperatures.

This paper discusses the methods used to measure convective heating in a large set of laboratory fires, and describes the gas temperature T_g and the local gas speed in the vicinity of the fuel particles, as functions of the distance from the flame front. Once these are known, approximate values for $\hbar$ can be calculated from an empirical equation based on a Reynolds–Nusselt number relationship (e.g. Incropera *et al*. 2007, eqn 7.44).

Materials and methods

Experimental facility

The experiments were conducted in a $3 \times 3 \times 26$ m wind tunnel at the USDA Forest Service Fire Sciences Laboratory in Missoula, Montana, USA. This facility allows control of fuel bed depth (δ), packing ratio, moisture content (M, the mass of water per unit dry mass of fuel), tunnel free stream wind speed (U), air temperature and relative humidity. The fuels were arranged on a 1-m wide fuel tray centred on the floor of the tunnel (Fig. 1). Strips of metal sheeting matching the fuel depth were placed along each side of the tray to reduce the inflow of air from the sides of the fuel bed, and to reflect radiant energy back into the

 10.1071/WF09021 1049-8001/10/030284

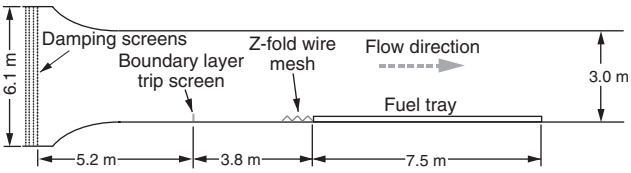

Fig. 1. A schematic of the wind tunnel used in the experiments (not to scale).

fuel array with the intention of mimicking a wider fire front. The metal sheeting was fastened to wire mesh, 0.25 m high and with a 12-mm grid, located along the two longitudinal sides of the fuel bed. A similar wire mesh arranged in Z-folds was located on the floor of the wind tunnel from wall to wall, beginning at the upwind edge of the fuel tray and continuing for ~1 m upstream. The height of the folds was adjusted to be the same as the fuel bed surface in order to simulate a longer reach of fuel and its resulting boundary layer. Without these modifications, the fire-front had a tendency to develop curvature, either leading in the centre (without the metal sheeting) or at the side (with the metal sheeting but without the Z-folds). Additional details about the facility and measurement methods can be found in Catchpole *et al*. (1998) and Rothermel and Anderson (1966).

Fuel beds, 1 m wide and 7.5 m long[A], were filled with fuel to a specified depth, packing ratio, and moisture content. Three different fuels, each with a unique surface area-to-volume ratio, were used. They consisted of aspen wood (*Populus tremuloides*) shavings, commonly referred to as excelsior or wood wool, and Ponderosa Pine (*Pinus ponderosa*) needles. The excelsior consisted of wood strands of fairly uniform rectangular cross-section, but variable in length, milled from aspen wood boles and packaged in bales. Two excelsior sizes were used, regular (~0.8 × 0.4 mm cross-section) and coarse (~2.5 × 0.8 mm cross-section). The excelsior was selected for its relatively consistent size, availability and ease with which it can be formed into a spatially uniform, randomly oriented fuel array. Fuel bed bulk density or packing ratio was adjusted by distributing the fuel at a predetermined loading (mass per unit area) and depth (Schuette 1965).

Before burning, fuels were pre-conditioned to the equilibrium moisture content corresponding to the relative humidity specified for the experiment (Schuette 1965). Fuel moisture was determined by analysing samples collected at the leading and trailing edge of the fuel array immediately before ignition.

The wind tunnel induction fan was located far upstream of the test section. Wind velocity in the tunnel was controlled by fixing the tunnel inlet fan speed that corresponded to the specified wind speed measured nominally 2 m above and 2 m upstream of the leading edge of the fuel bed, before the ignition of the fuel bed. This inlet fan speed was then maintained throughout the fire.

The ranges of fuel and environmental conditions are in Table 1. They were chosen to reflect the normal range of conditions when fires burn in natural accumulations of dead woody litter and grass – the pine needles represented pine forest litter and the excelsior represented fine shrubs and grasses. Of course, the range of possible experimental conditions was constrained by fuel array flammability and facility design limitations (see *Discussion*). There were 242 experiments burned under 163 different fuel and environmental conditions (referred to hereafter as sets).

Table 1. The range of conditions in the experimental burns using three fuel types
See *Glossary* for explanation of variables

Variable	Fuel type		
	Regular excelsior	Ponderosa pine needles	Coarse excelsior
s (m^{-1})	7600	5710	3090
β	0.001–0.040	0.020–0.063	0.005–0.090
δ (m)	0.08–0.15	0.03–0.08	0.03–0.15
M	0.03–0.21	0.03–0.28	0.03–0.26
U ($m\,s^{-1}$)	0.00–2.68	0.00–2.68	0.00–2.68

Instrumentation

Local fire front rate of spread was measured by recording the time of arrival and passage of the flame as indicated by photocells, spaced at 0.5-m intervals along the side of the fuel bed and 25 mm above the fuel surface, oriented to look horizontally across the fuel bed. Additional details are provided in Catchpole *et al*. (1998).

Air and fuel temperatures

All temperatures were measured using bare wire 0.13-mm diameter type K (chromel alumel) thermocouples (Omega Engineering, Inc., Stamford, CT, USA), with diameter at weld nominally 0.20 mm. For the excelsior fuels, the 'fuel temperature' thermocouple was located just below the fuel surface, in a small hole drilled through a piece of fuel. The excelsior fuel pieces used were nominally 4 cm long and of uniform cross-section. In the Ponderosa Pine needles, the thermocouple was threaded longitudinally through the centre of a needle. A 'gas temperature' thermocouple was placed 1–2 mm upstream from the fuel thermocouple without touching the fuel. Data from the thermocouples were sampled at 20 Hz.

Three strands of instrumented fuel were fastened at each end to two parallel 2.5-mm diameter steel wires, thus forming a 'ladder' with three rungs of fuel. Fig. 2 shows one of the rungs. The steel rods were nominally 4 cm apart and the rungs nominally 30 cm apart. The design and orientation of the thermocouple ladder was selected to minimise its influence on the local flow field along the fuel bed surface. Visual inspections of the fuel bed surface and ladder were made to ensure that the ladder did not compress the fuel bed or otherwise disturb its orientation. One or more ladders were placed with the long dimension aligned along the longitudinal surface of the fuel bed, positioned within 10 cm of the centre line of the bed, and with the first (most upstream) ladder rung located 4.7–5.5 m from the leading edge of the fuel bed.

The air and fuel temperatures from each thermocouple pair were plotted; the data from any pair were rejected if the fuel thermocouple tracked the air thermocouple too closely, indicating that the fuel thermocouple was not in good contact with the

[A]Beds burned under quiescent conditions (no wind) varied from 4.0 to 7.5 m in length, which is of the order of 100 times the flame zone depth.

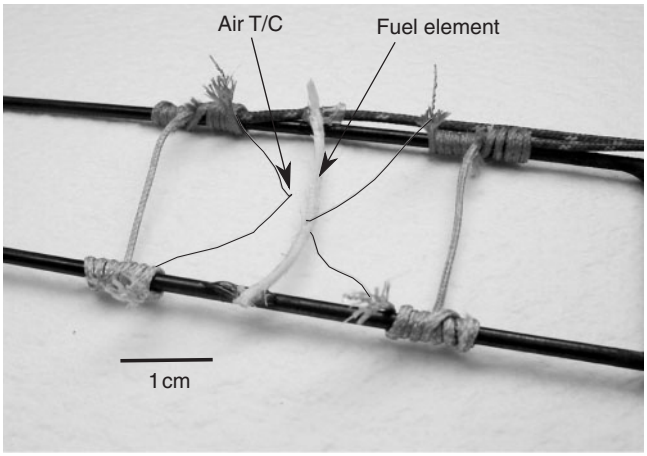

Fig. 2. A part of an instrumented ladder showing one of the 'rungs' of fuel with an embedded fuel thermocouple and an adjacent air thermocouple. The thermocouple wires, which are almost invisible in the original photo, have been redrawn.

Fig. 3. A kiel-static probe. Small gauge thermocouples positioned near the probe ports provide the temperature data needed in the pressure-to-velocity calculations. The wires, which are almost invisible in the original photo, have been redrawn.

fuel element and was primarily sensing the air temperature. As the temperature profiles from different rungs were quite variable due to the turbulent nature of the gas flow, the time-traces from the rungs of each fire were averaged over all fires burned under the same fuel and environmental conditions. Thus, the temperature data consists of sets of average air and fuel thermocouple profiles, each set corresponding to a unique combination of experimental conditions.

Gas flow

To measure surface wind velocity, kiel-static probes (McCaffrey and Heskestad 1976) were used. These were 12.7 mm in diameter and 25 mm in length, with an acceptance angle of ±30° (Fig. 3). Multiple probes were used in most experiments. The probes were placed at or just above the fuel bed surface, oriented to sense flow along the longitudinal axis of the fuel bed. They were located within 10 cm of the longitudinal centre line of the fuel bed, nominally 4.7–5.5 m from the leading edge of the fuel bed and positioned to minimise disturbance of the airflow directly upstream and in the vicinity of the thermocouple ladders.

Pressure readings from the probes were converted to velocity, using Bernoulli's equation, correcting for changes in air density based on temperature measured by a thermocouple near the probe opening. No correction was made for changes in local air humidity. All calculations were made using the standard properties of air at atmospheric pressure.

The kiel-static probe readings, which were sampled at 20 Hz, were smoothed with the robust local smoother loess (Cleveland *et al*. 1992). Smoothed traces from fires under the same fuel and environmental conditions were averaged.

Arguably, the dominant factors affecting the flow field along the surface of the fuel bed are the surface roughness and the presence of the flame front. Flow along the bed surface is dominated by boundary layer separation and wake interactions at the individual fuel particle scale. The ladder components were nominally of the same size or smaller than the fuel particles and were oriented along the principal plane formed by the ladder. The rungs were positioned to minimally affect the surface of the fuel bed. The assumption is made, therefore, that the ladder did not affect the surface flow field around the instrumented fuel strands and that the measured velocity approximates the dominant horizontal component of the local flow field.

Correcting the air thermocouple for radiation

The use of thermocouples to measure gas temperatures can be subject to considerable measurement uncertainty due to the loss or gain of energy by the thermocouple through radiant energy transfer (Shaddix 1998; Pitts *et al*. 2002). It was not possible to shield the air thermocouple as the air and fuel thermocouples needed to be relatively close and shielding would have changed the fluid boundary layer around the fuel element. Instead, the air thermocouple was corrected for the effect of radiation using an energy balance equation (Shaddix 1998). The thermocouple was assumed to be in thermal equilibrium, which is reasonable as the thermocouple will react much faster than the fuel to changes in the gas temperature. The thermocouple manufacturer specifies the time constant as 0.2 s, while a rough estimate indicates a nominal time constant of 1.6 s for the regular excelsior, and more for the other fuel particles.

The heat transfer coefficient used was that given in Collis and Williams (1959) for a cylinder, as in Shaddix (1998), using the diameter of the thermocouple wire for the characteristic length. The gas velocity consisted of the magnitude of the vector formed from horizontal and vertical components. The horizontal component used was calculated from the smoothed kiel probe trace, and the vertical component was the vertical buoyant velocity at the fuel bed surface given by R. Nelson, B. W. Butler and D. R. Weise (unpubl. data). For cases where no direct horizontal velocity measurements were available, a value equal to one half the wind tunnel free stream velocity was used (see *Discussion*). The film temperature required by the heat transfer coefficient relation was taken as 600 K near the flame when the difference between the air and fuel temperatures was more than 25 K, and 300 K far from the flame (the heat transfer coefficient is fairly insensitive to wind speed and film temperature and a sensitivity analysis showed that changing the values used had little effect). When available, measured values for the radiation source term were used (e.g. Butler 1993), otherwise, radiation was estimated from a regression equation using fuel load, wind speed, moisture

content, packing ratio and surface area-to-volume ratio as predictors. For zero-wind fires, a free convective heat transfer coefficient reported by Incropera *et al*. (2007, eqn 9.34) was used.

The thermocouples were located on the longitudinal centre line of the ladders, nominally 20 mm from the ladder sides (indicating a very small radiative exchange factor between the thermocouple bead and ladder wire), so radiative energy exchange between the ladder and thermocouples would have been minimal. Energy exchange by conduction along the thermocouple lead wires was minimised by using fine gauge wire (0.076 mm) for a distance of 30 mm from the thermocouple bead (Shaddix 1998).

Pitts *et al*. (2002) point out that the correction of thermocouple temperatures is subject to error due to the sometimes unknown parameters involved. Both the size of the corrections and the uncertainty in the corrections were minimised by using small sized (which reduces the absorption of radiant energy as compared with convection) shiny new thermocouples (which reduces the emission and absorption of radiant energy and enables a better estimate of them). The emissivity of the thermocouple was taken to be 0.65 (Hottel and Sarofim 1967, appendix to chapter 4). The small size also increases the response rate to variations in gas temperature. No correction for turbulence was made. Results of Marcelli *et al*. (2004, fig. 4) indicate that the correction is quite small near the fuel bed surface.

Results

Gas temperature profiles

The average measured fuel temperature profile and the corrected gas temperature profile from two sets of conditions (wind-driven and zero wind) are in Fig. 4. The gas temperature profile ahead of the fire can be modelled as a decreasing exponential function of the distance X from the flame:

$$T_g(X) = T_\infty + (T_{max} - T_\infty)\exp(-X/\xi) \qquad (2)$$

in a similar way to Pagni and Peterson (1973) and Koo *et al*. (2005). Here, $T_g(X)$ is the temperature of the gas at a distance X in front of the fire front and T_∞ is the ambient temperature of the surroundings. The parameter T_{max} is the gas temperature at the time of ignition of the fuel particle and the parameter ξ is a characteristic heating distance. This equation was fitted by non-linear least-squares to the corrected gas temperature for every set of fires giving estimates of T_{max} and ξ for each set. These estimates are given in the *Appendix* at the end of this paper. Examples of Eqn 2 fitted to gas temperature profiles are in Fig. 4. The fit of the exponential curves in Fig. 4 is typical: the fit is good in the wind-driven fires but quite poor for zero-wind fires. A possible reason for this is given in the *Discussion*.

Maximum gas temperature

Fig. 5 shows the maximum gas temperature T_{max} for each set as a function of wind tunnel speed U, together with the mean of T_{max} for each U. In this and the following figures, the values of U have been dithered (perturbed slightly) so that all sets are visible. For wind-driven fires, the values of T_{max} shown are those estimated from Eqn 2. For the zero-wind fires, for which Eqn 2 was a poor fit, this was replaced by the value of the corrected

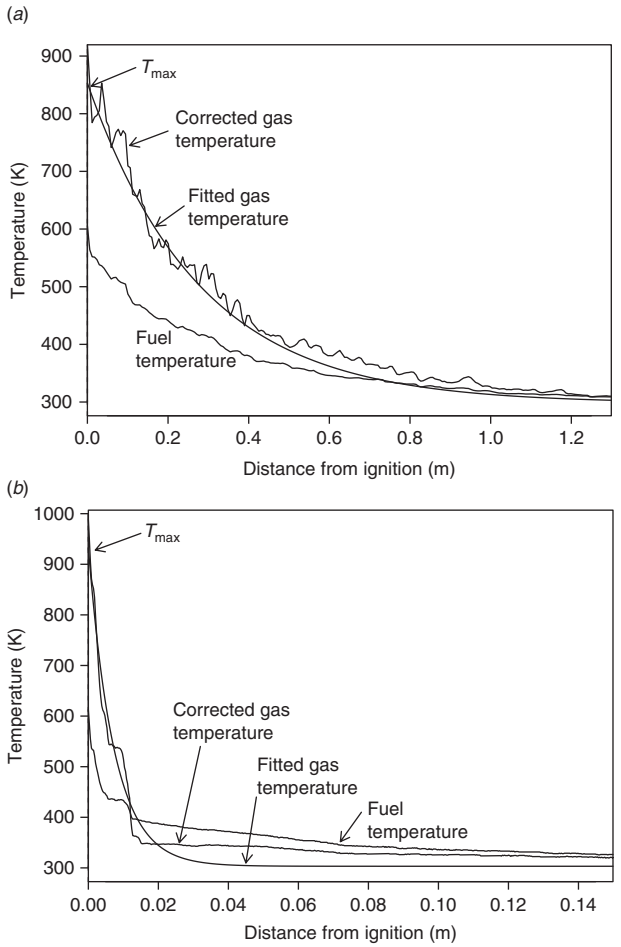

Fig. 4. The average measured fuel and corrected gas temperatures together with the exponential curve (Eqn 2, see text) fitted to the gas temperature, plotted against distance from the ignition interface. The averages are taken over all fires burned under the following conditions: (*a*) a wind-driven fire: set 219, $U = 2.68\,m\,s^{-1}$, $s = 3090\,m^{-1}$, $\beta = 0.01$, $\delta = 0.076\,m$, $M = 0.113$. The fitted exponential has $T_{max} = 864\,K$ and $\xi = 0.306\,m$; (*b*) a zero-wind fire: set 43, $U = 0$, $s = 3090\,m^{-1}$, $\beta = 0.01$, $\delta = 0.076\,m$, $M = 0.049$. The fitted exponential has $T_{max} = 933\,K$ and $\xi = 0.0073\,m$.

smoothed air temperatures at ignition. The mean value calculations were weighted, using the number of rungs as weights, so as to properly account for the differing quantity of information in the sets. For the same reason the following analyses were similarly weighted.

Fig. 5 shows T_{max} as relatively constant, except for very low and zero wind speed fires, where it increases noticeably. Fitting the curve:

$$T_{max} = a + b\exp(-cU) \qquad (3)$$

by nonlinear least-squares gives the parameter estimates $a = 863$ (18), $b = 316$ (36) and $c = 2.12$ (0.69). (Here and throughout the paper, figures in parentheses are s.e.) The fitted curve is in Fig. 5.

The scatter shown in Fig. 5 could be due to natural variation or might be due to dependence of T_{max} on the other environmental and fuel variables: packing ratio β, surface area-to-volume ratio (s), bed depth (δ) and fuel moisture content (M). Tests were

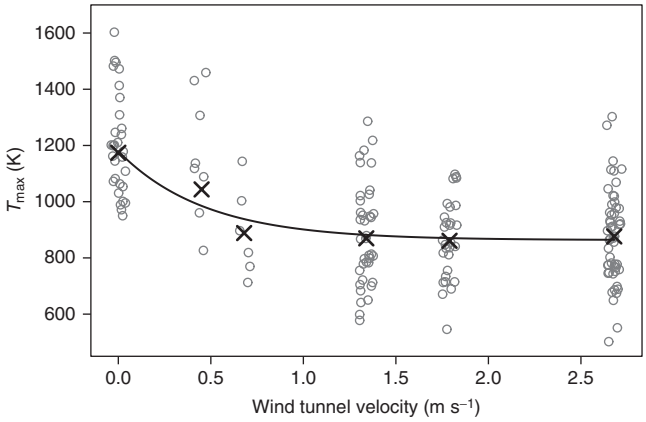

Fig. 5. The maximum gas temperature (T_{max}) together with its weighted mean value, shown as a cross, for each wind tunnel velocity. Wind values have been dithered for clarity in viewing. The fitted line is from Eqn 3 (see text).

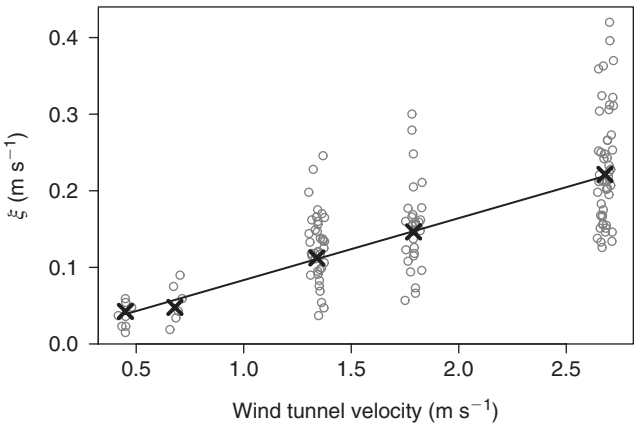

Fig. 6. The characteristic heating distance (ξ) with its weighted mean value (indicated by a cross) for each wind tunnel velocity. The fitted line is from Eqn 4 (see text).

performed for a linear effect of these variables, after allowing for wind dependence. To ensure that any possible lack of fit in Eqn 3 does not influence the analyses, a completely general wind dependence was fitted, then terms corresponding to the other variables were added.

There is a significant decrease in T_{max} with increasing β ($P = 0.007$) and with increasing M ($P = 0.006$). T_{max} decreases by 16 K (6 K) for each 0.01 increase in β and by 6 K (2 K) for each one percentage point increase in M. The other variables s, δ and fuel type (pine needles or excelsior) have no significant effect.

The residual s.d. of T_{max} after allowing for U is 148 K. Allowing also for M and β only decreases this to 142 K so the variation about the fitted line in Fig. 5 is a good indication of the natural variation.

The moisture damping effect is presumably due to water vapour in the flame decreasing its average temperature. A factor in the dependence on β may be increased resistance to air flow into the combustion region due to the increased fuel array density.

Characteristic heating distance

Fig. 6 shows the characteristic heating distance ξ, for each set as a function of wind tunnel speed U. Because of the poor fit of the exponential curve (Eqn 2) to zero-wind fires, only the wind-driven fires are analysed here. It is clear from the figure that the s.d. of ξ for each value of U increases markedly with U. A logarithmic transform of ξ stabilises the variance and this has been used in the analyses that follow. In such cases, the means shown in the figure are obtained from the transformed data and then reverse transformed. As with T_{max}, all calculations and analyses are weighted using the number of rungs as weights.

It is clear from Fig. 6 that the mean value of ξ increases with U in an almost linear fashion. Therefore, a regression

$$\xi = a + bU \qquad (4)$$

was fitted (in fact, the regression was of the form $\log \xi = \log(a + bU)$ and was fitted by nonlinear least-squares). This gives the estimates $a = 0.002$ (0.005), $b = 0.081$ (0.004) and the resulting fitted line is shown in Fig. 6. The variation in ξ with wind speed is much greater than that of T_{max}: ξ varies almost six-fold over the range of U values, as compared with only 1.4 for T_{max}, even though the zero-wind fires were excluded for ξ.

As with T_{max}, tests for additional influences on ξ were performed by first fitting a regression model with completely general wind dependence. There is a significant decrease in ξ with increasing β ($P = 0.0004$), and with increasing s ($P = 0.001$). The dependence is of the form $\xi \propto \beta^a s^b$ with $a = -0.15$ (0.03) and $b = -0.25$ (0.07). There is no significant influence from δ or M.

Because of the correlation between β and s (see *Discussion*), there is additional uncertainty in the above estimates and P values. A regression model which fits almost as well (residual s.d. = 0.322 as opposed to 0.320) is one in which ξ is regressed on the product $s\beta$, rather than on s and β separately. The decrease in ξ with $s\beta$ is of the form $\xi \propto (s\beta)^{-0.16}$. This ties in with physical theory, in particular, the conductivity of a bed of solid particles to a viscous fluid (the Carman–Kozeny equation, see Kay and Nedderman 1974). Note that the variation in ξ due to $s\beta$ is much less than that due to wind speed: over the range of $s\beta$ in the data, ξ varies (using the fitted equation) by a factor of 1.9.

An alternative physical explanation is possible. The effect of fuel load[B] $L = \rho_p \beta \delta$ is very similar to that of β, with $\xi \propto L^{-0.13}$. This effect could be explained in terms of fire-induced buoyancy, which increases with load and causes a decrease in the characteristic distance.

Gas velocity profiles

Fig. 7 shows surface velocity (U_{surf}) profiles typical of high-wind (Fig. 7*a*) and low-wind (Fig. 7*b*) fires, together with the gas temperature and fuel temperature profiles. In both cases shown, the 'set' consists of a single fire allowing the raw velocity curves to be shown as well as the smoothed ones.

At all wind speeds, three regions can be identified in the velocity profiles. In the first region, when the fire front is distance

[B]Values of fuel particle density (ρ_p) of 510 kg m^{-3} for the pine needles and 398 kg m^{-3} for the excelsior were used; see Catchpole *et al.* (1998).

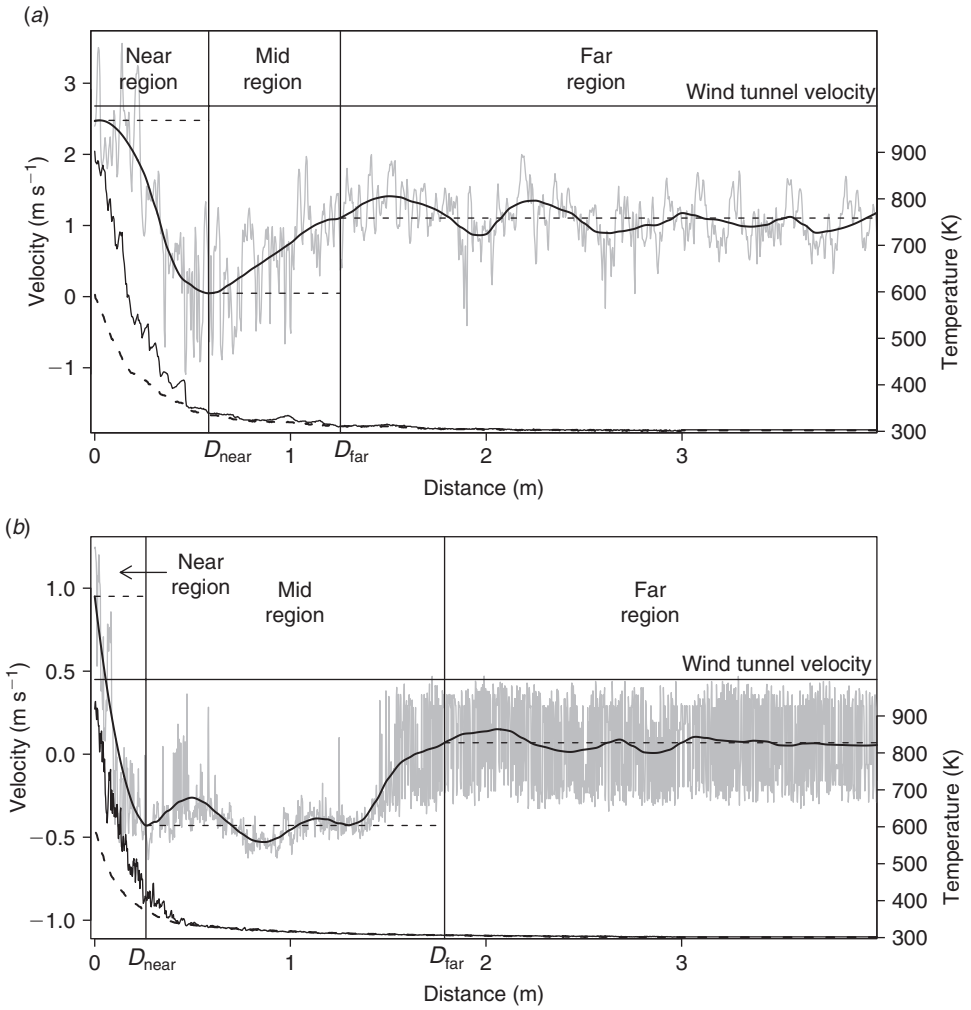

Fig. 7. The raw and smoothed surface gas velocities, plotted against distance from the ignition interface, together with the fuel (dashed line) and air (solid line) temperatures. The vertical lines show the divisions between the regions described in the text. The horizontal dotted lines show U_{max}, U_{min} and U_{far}. The conditions are (*a*) set 111, $U = 2.68\,m\,s^{-1}$, $M = 0.11$, $\beta = 0.02$, and (*b*) set 19, $U = 0.45\,m\,s^{-1}$, $M = 0.04$, $\beta = 0.005$. In both cases, $s = 7600\,m^{-1}$ and $\delta = 0.076\,m$.

D_{far} or more from a fuel element, the surface velocity remains relatively constant, with average value U_{far}. As the fire front approaches, the blocking effect of the flame causes the velocity to decrease to a minimum value U_{min}, which, in low-wind fires, is negative – a reversal of flow (Fig. 7*b*). This minimum, at distance D_{near}, tends to be just before the onset of convectional heating. In the third region, the velocity increases rapidly to a value U_{max}, as the fuel element ignites. U_{max} may reach, or even exceed, free-stream velocity. The algorithm for finding these values follows.

- The trace length was truncated at 4 m so that the results were not dominated by values far from ignition. For some of the low speed fires, in low and zero-wind conditions, a shorter distance had to be used because of limited data.
- A smoothed velocity profile, U_{surf}, was obtained from the raw surface velocity trace using loess (Cleveland *et al*. 1992) with a span equal to 0.6 divided by the trace length in metres (and so usually 0.15). Using cross-validation to calculate the span resulted in over-smoothing.
- U_{max} is defined as the maximum value of U_{surf} in the last metre before ignition.
- U_{min} is the local minimum (where the derivative is less than $0.0005\,m\,s^{-2}$) of U_{surf} closest to the fire-front. To cut out local minima that occur very close to ignition, this is replaced by the absolute minimum of U_{surf} in the last 1.5 m before ignition if this is at least $0.5\,m\,s^{-1}$ lower than the local minimum. D_{near} is the distance from ignition at which U_{min} occurs.
- D_{far} is the smallest distance from the flame, greater than $D_{near} + 0.25$, at which U_{surf} is greater than its average value over the region beyond D_{far}. U_{far} is the average of U_{surf} beyond D_{far}.

This algorithm failed if U_{surf} did not exhibit the characteristic behaviour of having a local maximum at a distance slightly greater than the location of the local minimum. In such cases,

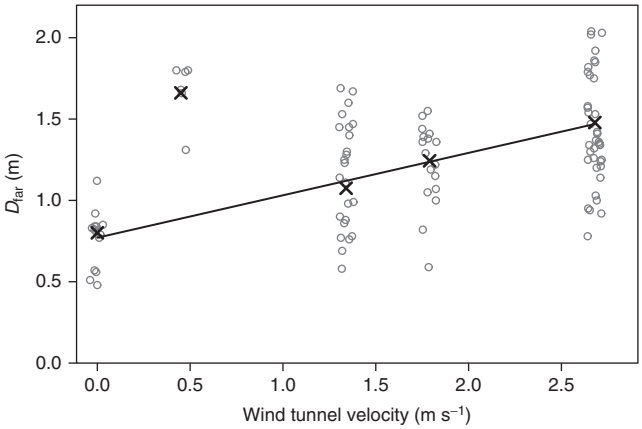

Fig. 8. D_{far} with its weighted mean value (indicated by a cross) for each wind tunnel velocity. The fitted line is from Eqn 5 (see text).

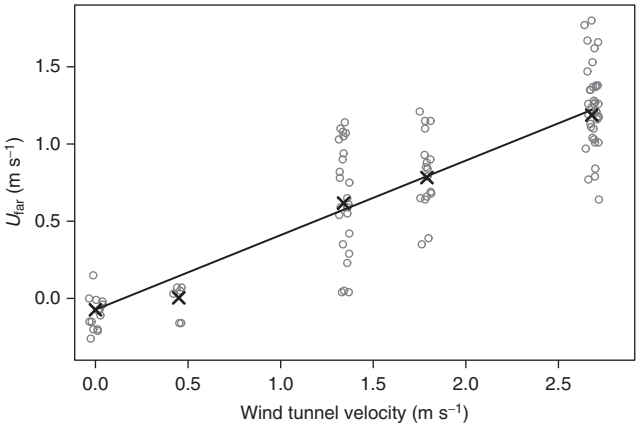

Fig. 9. U_{far}, the average gas velocity at the fuel bed surface, far from the fire with its weighted mean value (indicated by a cross) for each wind tunnel velocity. The fitted line is from Eqn 6 (see text).

D_{far} was estimated by eye. The values of U_{max}, U_{min}, U_{far}, D_{near} and D_{far} are tabulated in the *Appendix*.

Except for those involving U_{far}, all of the analyses that follow are performed using as weights the number of kiel probes for each set. Because U_{far} is an average over a length of time, the amount of information in each set depends not only on the number of kiel probes in each set, but also on the length of time over which the average is taken. For this reason, the analyses involving U_{far} use as weights the number of kiel probes multiplied by the length of time over which U_{far} is averaged. Kiel probe data are not available for the $U = 0.68\,m\,s^{-1}$ fires, and so these fires are missing from the following analyses.

Far from the flame

Fig. 8 shows D_{far} for each set as a function of wind tunnel speed U. It is clear from the figure that D_{far} increases with U in a roughly linear fashion except for notably high values for the low-wind fires at $0.45\,m\,s^{-1}$. These values were regarded as anomalous (see *Discussion*), and so a regression

$$D_{far} = a + bU \quad (5)$$

was fitted to the data from the remaining wind speeds. The estimates are $a = 0.77$ (0.07), $b = 0.26$ (0.03), and the resulting fitted line is in Fig. 8.

After allowing for wind dependence, the only environmental variable to significantly affect D_{far} is β, with a P-value of 0.007. D_{far} decreases by 0.05 m (0.02 m) for an increase in packing ratio of 0.01.

Fig. 9 shows the surface wind speed far from the fire, U_{far}, for each set, as a function of wind tunnel speed U. U_{far} increases with U in a roughly linear fashion except for notably low values for the low-wind fires at $0.45\,m\,s^{-1}$. Omitting these values (see *Discussion*) and fitting a regression:

$$U_{far} = a + bU \quad (6)$$

gives the estimates $a = -0.07$ (0.02), $b = 0.48$ (0.02) and the resulting fitted line is in Fig. 9. The fitting was by nonlinear least-squares after using a signed square root transform of U_{far} to diminish the heterogeneity of variance that is clearly evident in Fig. 9. The intercept a is very close to zero; in practical terms, in wind-aided fires, the average far surface wind speed was half the free stream speed. No other fuel and environmental variables significantly affected U_{far}.

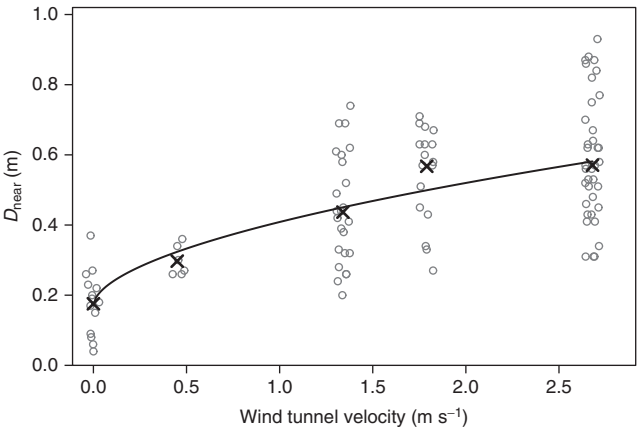

Fig. 10. D_{near} with its weighted mean value (indicated by a cross) for each wind tunnel velocity. The fitted line is from Eqn 7 (see text).

Middle region

In this region (Fig. 7), the surface wind speed drops from U_{far} to a minimum U_{min}, occurring at a distance D_{near} from the flame front. Fig. 10 shows D_{near}, for each set as a function of wind tunnel speed U. There appears to be a nonlinear relationship of the form

$$D_{near} = a + bU^c \quad (7)$$

and fitting this via nonlinear least-squares gives the estimates $a = 0.17$ (0.04), $b = 0.24$ (0.04) and $c = 0.55$ (0.14). There is slight evidence ($P = 0.02$) of a decrease in D_{near} with increasing β, or ($P = 0.03$) of an increase in D_{near} with increasing δ. Because of correlation between β and δ (see *Discussion*), it is not possible to determine which, if either, of these is a real physical effect.

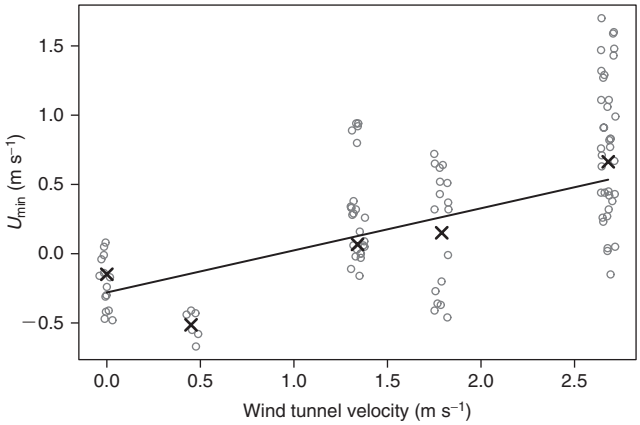

Fig. 11. U_{min} with its weighted mean value (indicated by a cross) for each wind tunnel velocity. The fitted line is from Eqn 8 (see text).

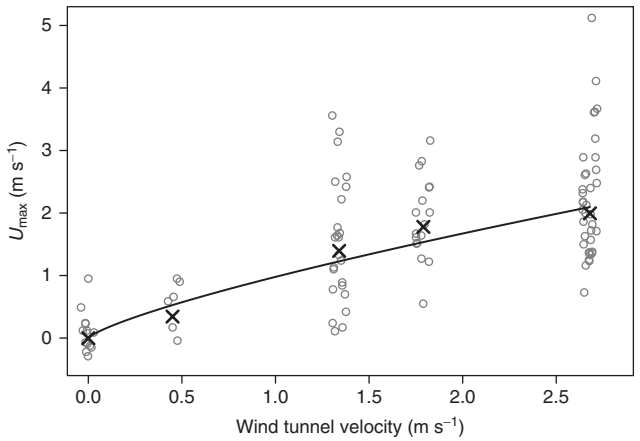

Fig. 12. U_{max} with its weighted mean value (indicated by a cross) for each wind tunnel velocity. The fitted line is from Eqn 9 (see text).

The relationship between U_{min} and U (Fig. 11) is similar to the relationship between U_{far} and U. There is a linear dependence of U_{min} on U except for the 0.45 m s^{-1} fires, all of which had substantial in-drafts (see *Discussion*). A regression on the other fires, of the form

$$U_{min} = a + bU \quad (8)$$

gives parameter estimates $a = -0.28$ (0.09) and $b = 0.30$ (0.05). As with U_{far}, these were obtained using nonlinear least-squares after a signed square root transform. There is evidence ($P = 0.003$) of a decrease in U_{min} with increasing fuel bed depth δ. An increase of 0.1m in fuel bed depth results in a decrease of 0.33 (0.11) in the signed square root of U_{min}. No other variables significantly affect U_{min}.

Near the flame

In this region, the velocity rises from a minimum to a maximum, U_{max}. The relationship between U_{max} and U is in Fig. 12. A regression of the form

$$U_{max} = a + bU^c \quad (9)$$

was fitted by nonlinear least-squares to the signed square root of U_{max}. The parameter estimates are $a = -0.002$ (0.01), $b = 0.98$ (0.12) and $c = 0.77$ (0.14). Note that the fitted curve passes almost exactly through the origin, as a is very close to zero. There is a significant ($P = 0.006$) increase in U_{max} with fuel moisture content, the signed square root of U_{max} increasing by 0.015 (0.005) for each percentage point increase in M. No other variables significantly affect U_{max}.

Discussion

The exponential model for gas temperature fits well for wind-aided fires but less well for zero-wind fires. For these fires, it is not possible, using an exponential model, to fit the temperature data well both near and far from the fire front. For the purpose of modelling convective heating, agreement close to the flame was felt to be more important and the method used achieves this. Good fit at all distances is possible using piecewise equations (not shown). A possible physical reason for this is that for zero-wind fires, the process of convective heating must be primarily by natural convection and turbulent diffusion rather than by forced convection, as noted by Pagni and Peterson (1973). As the flame front approaches, the air temperature near the fuel particle rises slowly but remains below the fuel temperature (giving convective cooling) until the fire is within a few centimetres of the flame front and then rises steeply (Fig. 4*b*). This indicates buoyancy-induced flow immediately before ignition and may be associated with gas-phase conduction adjacent to the flame front and possibly increased turbulence (Pagni and Peterson 1973).

At 0.45 m s^{-1}, the measured surface wind speed tended to be lower than predicted (Figs 9, 11). At this wind speed, a strong recirculation occurred along the ceiling of the wind tunnel. This did not occur at wind speeds greater than 1 m s^{-1} or during zero wind experiments. Such recirculation is a well recognised characteristic of flow through ducts with heated floors. During experiments, the wind tunnel fan was operated at constant speed resulting in a constant pressure inlet condition. We postulate that the recirculation along the ceiling causes a slightly increased pressure at the wind tunnel plenum inlet, which tends to block the inlet flow, resulting in a decreased velocity along the tunnel floor. Also, at 0.45 m s^{-1}, the shape of the surface flow profile tends to be such that our algorithm overestimates D_{far}. This is evident in Fig. 7*b* where D_{far} does not coincide with the sudden change in turbulence (as indicated by the amplitude of the oscillations of the raw velocity profile), and in Fig. 8, where the estimated D_{far} values are much greater than predicted. Additional modelling and experimental measurements are planned to further investigate this phenomenon. For these reasons, the 0.45 m s^{-1} fires were regarded as anomalous and were omitted from the analyses of D_{far}, U_{far} and U_{min}.

When correcting the air thermocouple readings for the effect of flame radiation, we used a gas velocity of one half of the wind tunnel free stream velocity in cases where there were no direct horizontal velocity measurements. This is compatible with our results for U_{far}; see comment following Eqn 6. This will therefore be a good approximation in the far region and is a reasonable approximation overall since it will be somewhat high in the mid region and somewhat low in the near region. Moreover, any introduced errors will be second order or smaller since this

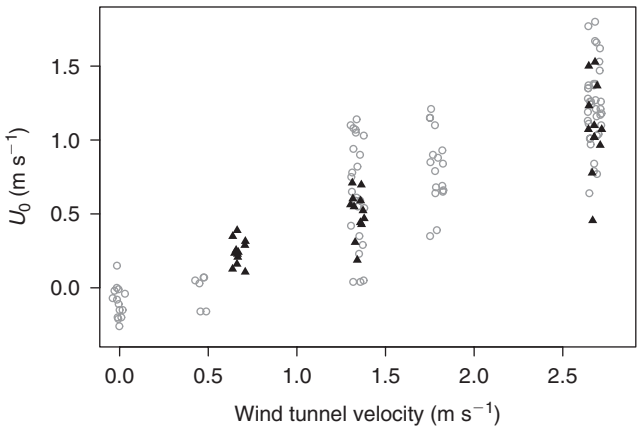

Fig. 13. The measured velocities at the fuel bed surface in the absence of fire (indicated by triangles) superimposed on a plot of U_{far} *v.* wind tunnel velocity (open circles).

is a correction of a correction and furthermore, the average convective heat transfer coefficient ($\hbar$) depends on the air velocity fairly weakly via a square root.

The finding that U_{far} is around half of the free stream wind speed leads to the question of whether this reduction is an effect of the fire or of the drag of the fuel bed. Currently, there is not enough data to allow this to be answered rigorously, but is clearly of interest to compare U_{far} with the surface wind U_0 in the absence of fire. Fig. 13 shows measured surface velocities in the absence of fire, U_0, superimposed on a plot, similar to Fig. 9, of U_{far} *v.* U. The strong overlap is consistent with the hypothesis that $U_{far} = U_0$, except for the low wind-speed fires, where there are in-drafts or recirculation in the presence of fire.

In an orthogonal study, the effect of any parameter can be estimated independently of the other parameters. However, it is not practicable to design experimental fires that both cover the range of fuel and environmental variables of practical interest and also form an orthogonal design. There are two reasons for this. First, in some conditions (for example, low fuel load and high moisture content), the fire will not burn. Second, in opposite conditions, with high load and low moisture content, fires are too intense and would damage the wind tunnel (or run the risk of escaping if burned in the field). This study covered a wide range of fuel and environmental parameters at the expense of orthogonality. However, most of the correlations between fuel and environmental parameters are quite low (Table 2), the only one of real concern being that between β and δ. As noted earlier, this results in uncertainty about which of these parameters affect D_{near}. The correlation between β and s also results in slight uncertainty as to how these variables affect ξ. None of the other conclusions are affected to any substantial degree by the correlations. In particular, note that correlations of all variables with U are uniformly low so that the effect of these variables can be estimated essentially independently of wind tunnel speed.

Conclusions

The primary objective of this paper was to characterise the gas temperature and flow that drive convective heating of fuel particles ahead of an advancing flame front. The authors could not find any studies in the literature that measure the gas temperature and flow ahead of a moving unconfined flame front. This paper attempts to fill this gap. Accurate simulation and prediction of convective energy transfer to the fuel array depends on such descriptions.

Temperature and velocity data collected in 242 experimental fires conducted in a large wind tunnel have been analysed. Based on the analysis, a general description has been given of the primary flow characteristics of the near surface flow over a porous array of fine fuels as a function of free stream wind speed, fuel parameters and proximity to the approaching flame front.

In wind-driven fires, the temperature of the mixture of air and pyrolysates ahead of the flame front decays exponentially from a maximum value at the flame front. This maximum value does not change with wind speed above $\sim$1 m s^{-1} and is somewhat higher at lower wind speeds. The maximum also decreases with increasing fuel packing ratio and moisture content. The characteristic decay length of the exponential is proportional to the wind speed and decays slightly with increasing fuel packing ratio and surface area-to-volume ratio.

Three flow regimes for surface wind flow are described. The first region consists of a region far from the flame front, characterised by relative constant flow. Surface velocity in this far region is proportional to the free stream wind speed: over our range of conditions, it was one half the free stream wind speed. The second region is a middle region characterised by a rapid decrease in surface wind speed to a minimum value, which in low-wind fires is a reversal of flow into the approaching flame front. The minimum speed is proportional to the free stream wind and decreases significantly with increasing fuel bed depth. In the third region near the fire front, the surface wind speed rises rapidly from the minimum value to a maximum value, close to the free-stream wind speed, at the fire front. The boundaries between the three regions move further from the flame front with increasing wind speed in a way which is only slightly affected by fuel geometry.

Table 2. Correlations between the fuel and environmental variables
See *Glossary* for explanation of variables

	U	s	β	δ	M
U	1.000	0.058	0.015	−0.015	0.022
s	0.058	1.000	0.192	−0.198	0.019
β	0.015	0.192	1.000	−0.371	0.020
δ	−0.015	−0.198	−0.371	1.000	−0.017
M	0.022	0.019	0.020	−0.017	1.000

Glossary of terms

D_{far} (m), the transition distance between the far and mid zones for convective heating.
D_{near} (m), the transition distance between the mid and near zones for convective heating.
$\hbar$ (kW m^{-2} K^{-1}), average convective heat transfer coefficient.
L (kg m^{-2}), fuel load – mass of fuel per plan area of fuel bed.
M, moisture content – mass of moisture per unit mass of dry fuel.

R ($m\,s^{-1}$), rate of spread – steady-state rate of advance of the fire front.
s (m^{-1}), surface area-to-volume ratio – surface area of fuel particle per unit volume of fuel particle.
T (K), particle temperature – temperature of the particles in a surface volume element.
T_∞ (K), ambient temperature – air temperature far from the flame front.
T_g (K), gas temperature – temperature of the air or gas surrounding the fuel particles.
T_{max} (K), maximum gas temperature – gas temperature at fuel ignition, as estimated from Eqn 2.
U ($m\,s^{-1}$), wind speed – free stream wind speed in the wind tunnel.
U_0 ($m\,s^{-1}$), wind speed at the fuel bed surface in the absence of fire.
U_{far} ($m\,s^{-1}$), value of U_{surf} far from the flame.
U_{min} ($m\,s^{-1}$), 'minimum' value of U_{surf} (see Algorithm).
U_{max} ($m\,s^{-1}$), value of U_{surf} near the flame front (see Algorithm).
U_{surf} ($m\,s^{-1}$), surface wind speed – gas velocity at the fuel bed surface.
X (m), distance from flame front – the distance of the surface volume element from the base of the flame.
β, packing ratio – volume of fuel per unit volume of fuel bed.
δ (m), fuel bed depth.
ρ_p ($kg\,m^{-3}$), particle density.
ξ (m), characteristic heating distance – characteristic decay length of the gas temperature, as estimated from Eqn 2.

Acknowledgements

This research was supported by funds from the Joint Fire Science Program and the US Forest Service. We thank Patricia Andrews for securing the funding. We also thank Bob Schuette, Paul Sopko, Merlin Brown, Kyle Shannon and Glen Morris for all their work constructing the fuel beds, setting up the instrumentation and processing the data.

References

Albini F (1985) A model for fire spread in wildland fuels by radiation. *Combustion Science and Technology* **42**, 229–258. doi:10.1080/00102208508960381

Butler BW (1993) Experimental measurements of radiant heat fluxes from simulated wildfire flames. In 'Proceedings of the 12th international conference on fire and forest meteorology', 26–28 October 1993, Jekyll Island, GA. (Eds JM Saveland, J Cohen) pp. 104–111. (Society of American Foresters: Bethesda, MD)

Catchpole WR, Catchpole EA, Rothermel RC, Morris GA, Butler BW, Latham DJ (1998) Rate of spread of free-burning fires in woody fuels in a wind tunnel. *Combustion Science and Technology* **131**, 1–37. doi:10.1080/00102209808935753

Clark JS (1996) Testing disturbance theory with long-term data: alternative life-history solutions to the distribution of events. *American Naturalist* **148**, 976–996. doi:10.1086/285967

Cleveland WS, Grosse E, Shyu WM (1992) Local regression models. In 'Statistical models in S'. (Eds JM Chambers, TJ Hastie) Ch. 8, pp. 309–373. (Wadsworth & Brooks/Cole: Pacific Grove, CA, USA)

Collis D, Williams M (1959) Two-dimensional convection from heated wires at low Reynolds numbers. *Journal of Fluid Mechanics* **6**, 357–384. doi:10.1017/S0022112059000696

Hottel HC, Sarofim AF (1967) 'Radiative transfer.' (McGraw-Hill: New York)

Incropera FP, DeWitt DP, Bergman TL, Adrienne AS (2007) 'Fundamentals of heat and mass transfer.' 6th edn. (Wiley: New York)

Kay JM, Nedderman RM (1974) 'An introduction to fluid mechanics and heat transfer.' (Cambridge University Press: Cambridge, UK)

Koo E, Pagni P, Woycheese J, Stephens S, Weise DR, Huff J (2005) A simple physical model for forest fire spread rate. In 'Fire safety science. Proceedings of the 8th international symposium', 18–23 September 2005, Beijing, China. pp. 851–862. (International Association for Fire Safety Science: London)

Linn R, Winterkamp J, Edminster C, Colman J, Steinzig M (2003) Modeling interactions between fire and atmosphere in discrete element fuel beds. In 'Proceedings of the 5th symposium on fire and forest meteorology', 16–20 November 2003, Orlando, FL. Paper J2.2. (American Meteorological Society: Washington, DC)

Marcelli T, Santoni PA, Simeoni A, Leoni E, Porterie B (2004) Fire spread across pine needle fuel beds: characterization of temperature and velocity distributions within the fire plume. *International Journal of Wildland Fire* **13**, 37–48. doi:10.1071/WF02065

McCaffrey BJ, Heskestad G (1976) A robust bidirectional low-velocity probe for flame and fire application. *Combustion and Flame* **26**, 125–127. doi:10.1016/0010-2180(76)90062-6

Mell W, Manzello S, Maranghides A (2006) Numerical modeling of fire spread through trees and shrubs. In 'Proceedings of the Vth international conference on forest fire research, Figueira da Foz, Portugal'. (Ed. DX Viegas) pp. 1–12. (Elsevier: London)

Morvan D, Dupuy J (2004) Modeling the propagation of a wildfire through a mediterranean shrub using a multiphase formulation. *Combustion and Flame* **138**, 199–210. doi:10.1016/J.COMBUSTFLAME.2004.05.001

Pagni P, Peterson T (1973) Flame spread through porous fuels. In 'Proceedings of the 14th international symposium on combustion'. pp. 1099–1106. (The Combustion Institute: Pittsburgh, PA)

Pitts WM, Braun E, Peacock RD, Mitler H, Johnsson EL, Reneke PA, Blevins LG (2002) Temperature uncertainties for bare-bead and aspirated thermocouple measurements in fire environments. In 'Thermal measurements: the foundation of fire standards'. (Eds LA Gritzo, NJ Alvares) (ASTM International: West Conshohocken, PA)

Raupach M, Shaw R (1982) Averaging procedures for flow within vegetation canopies. *Boundary-Layer Meteorology* **22**, 79–90. doi:10.1007/BF00128057

Rothermel RC (1972) A mathematical model for predicting fire spread in wildland fuels. USDA Forest Service, Intermountain Forest and Range Experimental Station, Research Paper INT-115. (Ogden, UT)

Rothermel RC, Anderson HE (1966) Fire spread characteristics determined in the laboratory. USDA Forest Service, Intermountain Forest and Range Experimental Station, Research Paper INT-30. (Ogden, UT)

Schuette RD (1965) Preparing reproducible pine needle fuel beds. USDA Forest Service, Intermountain Forest and Range Experimental Station, Research Note INT-36. (Ogden, UT)

Seron FJ, Gutierrez D, Magallon J, Ferragut L, Assensio MI (2005) The evolution of wildland forest fire front. *The Visual Computer* **21**, 152–159.

Shaddix CR (1998) Practical aspects of correcting thermocouple measurements for radiation loss. In 'Proceedings of 1998 Fall Meeting of the Western States Section of The Combustion Institute', 26–27 October 1998, Seattle, WA. (The Combustion Institute: Pittsburgh, PA)

Manuscript received 21 February 2009, accepted 21 October 2009

Appendix

The table below shows averages over each set of fires (with constant fuel and environmental conditions), of the quantities used in the paper. A bar denotes the average value in a set, and σ denotes a s.d. Thus, for example, $\overline{R}$ is the average rate of spread, and σ_R is the s.d. of rate of spread over a set of conditions. Also shown are N_f (number of fires), N_r (rungs) and N_{kp} (kiel-static probes) in each set.

Some of the rows in the data table do not have entries for some variables, in particular for gas flow variables, because the traces were anomalous. Some sets consist of only one burn experiment; therefore s.d. for moisture content or rate of spread could not be calculated.

Set	s	β	δ	U	$\overline{M}$	σ_M	$\overline{R}$	σ_R	N_f	N_r	$T_{\max}$	ξ	N_{kp}	D_{far}	D_{near}	U_{far}	$U_{\min}$	$U_{\max}$
1	3092	0.020	0.076	1.34	0.055	0.001	0.060	0.001	6	17	944	0.134	9	0.86	0.44	0.59	−0.02	1.64
2	3092	0.020	0.152	2.68	0.073	0.002	0.083	0.006	2	6	775	0.311	0					
3	7596	0.005	0.076	2.68	0.039		0.228		1	1	770	0.151	0					
4	7596	0.005	0.152	2.68	0.045		0.202		1	3	803	0.212	2	1.75	0.56	1.37	0.02	1.36
5	7596	0.005	0.152	1.34	0.050		0.144		1	3	599	0.228	2	1.47	0.62	1.03	0.05	2.42
6	3092	0.010	0.076	2.68	0.054	0.000	0.129	0.002	3	9	1116	0.253	5	1.57	0.70	1.19	0.44	2.32
7	7596	0.020	0.076	1.34	0.032	0.004	0.069	0.002	2	4	932	0.097	2	0.69	0.28	0.94	0.29	1.61
9	5710	0.063	0.076	1.34	0.066		0.018		1	3	721	0.091	2	0.77	0.24	0.78	0.28	1.13
10	3092	0.010	0.152	1.34	0.072	0.006	0.078	0.001	3	9	809	0.133	1					
11	3092	0.020	0.076	2.68	0.060	0.002	0.090	0.001	5	11	912	0.212	3	1.34	0.62	1.47	1.43	3.19
12	3092	0.020	0.076	1.79	0.062		0.058		1	3	818	0.159	1					
13	3092	0.020	0.076	1.79	0.032		0.071		1	3	811	0.178	1	1.19	0.43	0.88	0.64	1.82
14	7596	0.020	0.076	2.68	0.057	0.002	0.091	0.004	3	8	979	0.151	2	1.32	0.75	0.79	1.06	1.37
15	5710	0.020	0.076	1.79	0.060		0.037		1	1	987	0.123	0					
16	7596	0.010	0.076	1.79	0.080	0.003	0.111	0.002	2	5	924	0.166	0					
18	3092	0.030	0.076	1.34	0.058		0.046		1	3	778	0.118	2	0.76	0.26	0.59	−0.03	0.84
19	7596	0.005	0.076	0.45	0.042		0.038		1	2	1459	0.023	2	1.79	0.26	0.07	−0.43	0.95
20	5710	0.020	0.076	2.68	0.062	0.001	0.062	0.001	3	7	926	0.202	4	1.79	0.87	1.28	0.76	2.05
22	3092	0.020	0.152	1.34	0.079	0.002	0.047	0.003	2	6	957	0.117	0					
23	3092	0.030	0.076	1.34	0.037		0.056		1	2	1026	0.149	1					
24	7596	0.020	0.076	1.34	0.173		0.039		1	2	879	0.121	1	0.98	0.32	0.23	−0.16	1.24
25	5710	0.021	0.025	2.68	0.100		0.042		1	3	961	0.420	1					
26	7596	0.005	0.076	1.34	0.035		0.113		1	1	1218	0.160	0					
27	3092	0.010	0.152	2.68	0.237	0.001	0.069	0.002	2	4	976	0.250	1	1.20	0.87	1.66	0.77	5.12
28	3092	0.030	0.025	2.68	0.040	0.002	0.086	0.001	3	8	1069	0.203	6	1.41	0.41	0.77	0.83	1.82
30	3092	0.010	0.076	2.68	0.218		0.079		1	3	1022	0.248	1	2.03	0.77	1.18	0.99	3.67
31	3092	0.010	0.076	1.79	0.242		0.049		1	3	925	0.177	1	1.38	0.68	0.64	0.52	2.83
32	3092	0.030	0.076	1.34	0.251		0.020		1	3	797	0.138	1	1.23	0.60	1.05	0.94	3.14
33	3092	0.030	0.076	1.79	0.053		0.048		1	2	917	0.108	1	0.59	0.34	0.68	−0.37	2.20
34	3092	0.030	0.076	2.68	0.040	0.001	0.078	0.002	2	5	931	0.198	2	1.24	0.45	1.17	1.48	4.11
35	3092	0.030	0.152	2.68	0.043		0.078		1	3	677	0.322	1	1.35	0.93	1.53	1.59	3.62
36	3092	0.020	0.076	2.68	0.029		0.085		1	2	932	0.134	1	1.37	0.31	1.21	0.82	1.72
37	3092	0.030	0.025	1.34	0.048		0.043		1	3	1183	0.106	1	1.60	0.69	0.35	0.16	2.22
38	3092	0.010	0.025	1.34	0.032		0.046		1	3	1138	0.118	1	1.30	0.38	0.55	0.94	1.68
39	3092	0.010	0.025	2.68	0.042		0.069		1	3	1302	0.138	1	2.02	0.88	1.26	1.29	2.63
40	3092	0.020	0.076	1.34	0.036		0.050		1	2	814	0.111	1	1.25	0.39	1.07	0.32	1.77
41	3092	0.010	0.152	2.68	0.031		0.133		1	2	1145	0.266	1	1.82	0.86	1.37	0.63	1.86
42	3092	0.020	0.076	1.34	0.068	0.004	0.066	0.002	4	11	867	0.115	1	1.14	0.49	0.42	−0.11	0.24
43	3092	0.010	0.076	0.00	0.049		0.006		1	3	989		2	0.56	0.20	−0.01	0.08	0.08

(*Continued*)

Set	s	β	δ	U	$\overline{M}$	σ_M	$\overline{R}$	σ_R	N_f	N_r	$T_{\max}$	ξ	N_{kp}	D_{far}	D_{near}	U_{far}	$U_{\min}$	$U_{\max}$
44	3092	0.010	0.076	1.34	0.040		0.077		1	2	1163	0.156	1	1.45	0.61	1.10	0.34	3.56
45	3092	0.030	0.076	0.00	0.106	0.003	0.007	0.000	4	20	1210		6	0.79	0.22	−0.15	−0.17	−0.15
46	3092	0.010	0.076	0.00	0.193		0.004		1	2	1603		1	0.51	0.26	−0.07	−0.16	0.49
47	3092	0.030	0.152	2.68	0.253	0.003	0.025	0.001	2	6	759	0.166	2	0.92	0.34	1.26	0.43	1.71
49	3092	0.010	0.152	2.68	0.079		0.112		1	2	877	0.242	1	1.53	0.67	1.80	0.32	2.40
50	3092	0.030	0.076	1.79	0.190	0.010	0.024	0.000	2	5	848	0.137	2	1.07	0.58	0.65	−0.01	2.42
51	3092	0.030	0.076	2.68	0.221	0.004	0.036	0.000	2	6	686	0.273	2	1.21	0.62	1.21	0.67	2.69
52	3092	0.010	0.152	2.68	0.047		0.106		1	9	953	0.221	3	1.42	0.57	1.03	−0.15	1.38
53	3092	0.020	0.152	1.79	0.050		0.058		1	3	546	0.205	1					
54	3092	0.010	0.076	1.79	0.035		0.077		1	3	1084	0.126	1	1.36	0.63	0.35	−0.41	1.61
55	3092	0.020	0.076	0.00	0.028		0.010		1	3	1473		2	0.57	0.17	0.00	−0.01	0.24
57	3092	0.030	0.076	0.00	0.037		0.007		1	2	1145		2					
58	3092	0.010	0.076	0.00	0.109	0.001	0.005	0.000	2	6	1082		3					
59	3092	0.030	0.076	0.00	0.214		0.005		1	3	1108		1	0.48	0.04	−0.15	−0.24	0.95
60	3092	0.010	0.025	2.68	0.069		0.121		1	3	999	0.363	1					
61	3092	0.010	0.152	2.68	0.055	0.001	0.113	0.002	4	12	990	0.212	7	1.77	0.62	1.26	0.23	1.63
62	3092	0.020	0.076	2.68	0.103		0.103		1	2	1046	0.175	0					
64	5710	0.063	0.076	0.00	0.064	0.001	0.004	0.001	2	5	950		2	0.83	0.23	−0.02	−0.04	0.12
65	5710	0.032	0.076	0.00	0.067		0.006		1	2	1239		1					
66	5710	0.021	0.025	2.68	0.029		0.085		1	2	1272	0.252	2	0.78	0.52	1.13	1.47	2.38
67	5710	0.060	0.051	1.34	0.044		0.019		1	2	1286	0.037	1	0.90	0.44	0.75	0.33	0.78
68	5710	0.021	0.076	1.79	0.246		0.018		1	3	837	0.279	1	1.36	0.67	0.66	0.32	3.16
69	5710	0.021	0.076	2.68	0.275	0.006	0.035	0.000	2	5	674	0.396	2	0.95	0.56	1.77	1.70	2.89
70	5710	0.063	0.025	2.68	0.265		0.012		1	2	551	0.359	1	0.94	0.43	1.01	1.27	2.61
71	5710	0.021	0.025	2.68	0.262		0.018		1	2	765	0.243	1	1.14	0.51	1.62	1.60	2.89
72	5710	0.063	0.025	2.68	0.114		0.030		1	3	782	0.168	0					
73	5710	0.063	0.025	2.68	0.034	0.000	0.058	0.006	2	5	1114	0.156	2	1.47	0.53	0.97	0.91	1.16
74	5710	0.063	0.025	2.68	0.067	0.001	0.046	0.002	3	7	649	0.183	4	1.30	0.63	1.01	0.91	2.00
76	5710	0.021	0.076	1.34	0.102	0.005	0.030	0.001	3	8	1041	0.090	3	0.78	0.41	0.29	0.06	0.70
77	5710	0.021	0.076	0.00	0.065		0.004		1	3	1202		2	0.82	0.09	−0.08	−0.14	−0.07
78	5710	0.063	0.076	2.68	0.056		0.029		1	3	777	0.133	2					
79	5710	0.021	0.076	1.34	0.166		0.018		1	3	755	0.144	1	0.88	0.58	0.61	0.03	1.33
80	5710	0.063	0.076	1.34	0.160		0.004		1	3	650	0.147	1	1.11	0.20	1.14	0.80	1.61
81	5710	0.063	0.076	2.68	0.264		0.009		1	1	502	0.213	1					
83	3092	0.030	0.076	1.79	0.033		0.050		1	3	863	0.096	1	1.00	0.27	0.84	0.37	2.01
84	3092	0.010	0.152	2.68	0.249		0.071		1	3	921	0.312	1	1.36	0.84	1.04	0.38	3.61
87	3092	0.010	0.076	1.34	0.236		0.046		1	3	1003	0.170	1	0.99	0.74	0.54	0.26	2.58
88	3092	0.020	0.076	1.34	0.045		0.061		1	3	705	0.135	0					
89	3092	0.020	0.076	1.34	0.045		0.061		1	3	952	0.198	0					
90	3092	0.020	0.076	1.34	0.045		0.061		1	3	961	0.125	0					
91	3092	0.020	0.076	1.34	0.045		0.061		1	3	713	0.137	0					

102	7596	0.002	0.076	1.79	0.097		0.207		1	3	715	0.160	1					
103	7596	0.001	0.076	1.79	0.105		0.163		1	2	981	0.073	1					
104	7596	0.020	0.076	1.79	0.139		0.065		1	3	910	0.115	1	1.15	0.57	0.93	0.51	2.41
105	7596	0.020	0.076	1.79	0.057	0.004	0.062	0.001	3	7	1089	0.066	2					
107	7596	0.005	0.102	0.00	0.059		0.016		1	2	1413		0					
108	7596	0.020	0.076	1.79	0.182		0.043		1	3	713	0.169	1	1.29	0.57	0.90	−0.36	2.76
109	7596	0.020	0.076	2.68	0.206		0.062		1	3	1110	0.156	1					
110	7596	0.020	0.076	1.79	0.116		0.052		1	3	1097	0.094	1	1.22	0.63	0.69	−0.46	1.22
111	7596	0.020	0.076	2.68	0.113		0.076		1	2	958	0.214	1	1.25	0.58	1.10	0.05	2.48
112	7596	0.020	0.076	1.79	0.032		0.075		1	3	715	0.148	1	1.41	0.33	0.39	−0.20	0.55
113	7596	0.020	0.076	2.68	0.027		0.112		1	3	867	0.146	1	1.86	0.82	0.84	0.04	1.23
115	7596	0.020	0.076	0.00	0.038	0.004	0.015	0.001	2	5	1054		2					
116	7596	0.020	0.076	0.00	0.168		0.009		1	3	1072		1	0.92	0.08	−0.20	−0.47	−0.22
118	7596	0.005	0.152	0.45	0.030		0.034		1	3	1307	0.015	2	1.68	0.34	0.03	−0.41	0.17
121	7596	0.010	0.076	1.79	0.123		0.112		1	3	690	0.156	0					
122	7596	0.040	0.076	1.79	0.069	0.006	0.042	0.001	2	6	1082	0.057	0					
123	7596	0.020	0.076	1.34	0.190		0.038		1	2	578	0.246	1					
125	3092	0.030	0.076	0.00	0.062		0.008		1	3	1064		1					
128	3092	0.010	0.159	0.00	0.116		0.010		1	3	1031		1					
129	3092	0.030	0.152	1.34	0.070	0.002	0.034	0.001	4	11	1022	0.054	3	1.45	0.52	0.90	0.00	0.89
130	3092	0.030	0.152	0.00	0.093		0.011		1	3	1261		1	0.85	0.18	−0.04	−0.48	0.09
131	3092	0.030	0.076	1.34	0.239		0.020		1	2	936	0.047	0					
132	3092	0.010	0.076	1.34	0.256		0.043		1	3	783	0.083	2	1.28	0.45	0.82	0.92	3.30
136	3092	0.020	0.076	0.00	0.121	0.002	0.009	0.000	2	3	971		0					
201	3092	0.010	0.076	1.79	0.105		0.096		1	4	993	0.155	1	1.39	0.51	1.21	−0.27	1.52
202	3092	0.005	0.076	1.79	0.105		0.117		1	5	834	0.248	1	1.05	0.60	1.10	0.62	1.64
203	3092	0.005	0.076	1.79	0.063	0.003	0.091	0.003	2	9	755	0.211	4	1.44	0.69	1.15	0.72	2.01
204	3092	0.005	0.076	2.68	0.066	0.001	0.147	0.001	2	7	752	0.228	4	1.25	0.31	1.35	1.32	2.18
205	3092	0.005	0.076	0.45	0.055	0.001	0.022	0.001	2	11	1118	0.054	4					
206	3092	0.005	0.076	0.00	0.068		0.005		1	5	1482		2	0.84	0.27	−0.11	−0.42	−0.09
207	3092	0.005	0.152	0.00	0.044		0.008		1	6	1247		2	0.77	0.15	−0.20	−0.41	−0.12
208	7596	0.002	0.076	0.45	0.041		0.044		1	5	1089	0.036	0					
209	7596	0.002	0.076	2.68	0.058	0.007	0.293	0.004	2	12	909	0.324	4	1.92	0.64	1.38	1.11	1.98
210	7596	0.002	0.076	0.45	0.051		0.043		1	5	1431	0.023	2	1.80	0.27	−0.16	−0.58	0.90
211	7596	0.002	0.076	1.79	0.070		0.167		1	6	734	0.300	2					
212	7596	0.002	0.076	1.79	0.069	0.000	0.162	0.016	2	10	945	0.148	4					
214	3092	0.005	0.152	0.45	0.075	0.000	0.029	0.003	2	12	960	0.059	4	1.31	0.36	0.07	−0.67	−0.04
215	3092	0.005	0.152	1.79	0.077	0.003	0.101	0.005	2	12	917	0.155	2	1.52	0.71	1.15	0.32	1.67
216	3092	0.005	0.152	2.68	0.074	0.002	0.142	0.003	2	15	1020	0.146	4	1.85	0.48	1.67	0.45	1.33
217	3092	0.005	0.152	0.00	0.070		0.008		1	6	1162		2	0.81	0.19	−0.21	−0.31	0.12
218	3092	0.010	0.076	1.79	0.126	0.001	0.071		2	12	855	0.162	4	0.82	0.45	0.85	0.65	1.51
219	3092	0.010	0.076	2.68	0.113	0.004	0.116	0.005	3	20	864	0.306	5	1.58	0.57	1.35	1.11	2.17

(*Continued*)

Set	s	β	δ	U	$\overline{M}$	σ_M	$\overline{R}$	σ_R	N_f	N_r	$T_{\max}$	ξ	N_{kp}	D_{far}	D_{near}	U_{far}	$U_{\min}$	$U_{\max}$
220	3092	0.010	0.076	0.45	0.117	0.001	0.021	0.000	2	11	1137	0.048	4	1.66	0.30	−0.16	−0.55	0.66
221	3092	0.010	0.076	0.00	0.118	0.002	0.005		2	11	995		4	1.12	0.06	−0.26	−0.30	−0.29
222	3092	0.030	0.076	0.45	0.113	0.002	0.013	0.000	3	17	827	0.037	6	1.80	0.26	0.05	−0.44	0.59
223	3092	0.030	0.076	1.79	0.127	0.002	0.034	0.001	2	12	671	0.159	4	1.55	0.63	0.79	0.43	1.27
224	3092	0.030	0.076	2.68	0.125		0.042		1	6	834	0.155	2	1.00	0.31	1.16	0.83	1.36
225	3092	0.030	0.076	2.68	0.070	0.008	0.054	0.003	2	16	897	0.233	2	1.54	0.46	1.11	0.71	1.50
226	3092	0.010	0.076	1.34	0.047		0.071		1	11	1139	0.095	1					
227	3092	0.010	0.076	0.67	0.064		0.041		1	8	1003	0.075	1					
228	3092	0.030	0.076	0.68	0.063		0.030		1	10	713	0.090	1	1.54	0.26	0.01	−0.11	0.12
229	3092	0.030	0.076	1.34	0.065		0.049		1	12	683	0.120	1	1.67	0.32	0.05	0.09	0.42
230	7596	0.010	0.076	1.34	0.065		0.066		1	12	700	0.099	1	1.40	0.26	0.04	0.00	0.17
231	7596	0.010	0.076	0.68	0.076		0.046		1	10	897	0.059	1					
232	7596	0.030	0.076	0.68	0.075		0.028		1	11	770	0.034	1					
233	7596	0.010	0.076	2.68	0.071		0.145		1	9	745	0.213	1					
234	7596	0.030	0.076	1.34	0.072		0.048		1	8	869	0.076	1	0.58	0.33	0.04	0.06	0.11
235	7596	0.030	0.076	2.68	0.075		0.088		1	9	856	0.126	1					
236	3092	0.060	0.076	0.68	0.063		0.017		1	7	819	0.043	1					
237	7596	0.005	0.076	1.34	0.067		0.096		1	8	785	0.162	1					
238	7596	0.005	0.076	2.68	0.070		0.203		1	7	748	0.266	1					
239	3092	0.060	0.076	1.34	0.066		0.029		1	7	641	0.175	1	1.69	0.42	0.65	0.89	1.10
240	3092	0.060	0.076	2.68	0.066		0.058		1	9	743	0.207	1					
241	3092	0.090	0.076	1.34	0.075		0.023		1	11	807	0.069	1					
242	3092	0.090	0.076	2.68	0.068		0.066		1	11	689	0.304	1					
243	3092	0.090	0.076	0.68	0.084		0.011		1	9	1144	0.019	1					
245	3092	0.020	0.076	1.34	0.145		0.035		1	8	799	0.165	1					
251	3092	0.010	0.076	0.00	0.084		0.005		1	4	1179		1					
255	3092	0.030	0.076	0.00	0.087		0.007		1	3	1309		2					
264	3092	0.005	0.076	0.00	0.069		0.003		1	4	1502		1					
265	3092	0.010	0.152	0.00	0.070		0.009		1	4	1371		1					
270	3092	0.030	0.152	0.00	0.080		0.010		1	2	1202		0					
275	3092	0.005	0.152	0.00	0.082		0.007		1	3	1199		1					
281	3092	0.010	0.025	0.00	0.066		0.003		1	3	1001		1					
306	3092	0.010	0.076	2.68	0.050	0.001	0.124	0.004	2	5	774	0.218	2	1.03	0.53	1.27	0.42	1.57
310	3092	0.010	0.152	1.34	0.046	0.003	0.084	0.002	2	2	948	0.166	1	1.53	0.69	1.08	0.38	2.50
325	5710	0.021	0.025	2.68	0.070		0.093		1	3	777	0.370	1					
335	3092	0.030	0.152	2.68	0.068		0.062		1	2	870	0.195	1	1.26	0.43	1.38	0.27	1.25
343	3092	0.010	0.076	0.00	0.053		0.005		1	1	1495		1	0.84	0.37	0.15	0.05	0.23
373	5710	0.063	0.025	2.68	0.047		0.051		1	3	698	0.168	3	1.34	0.41	0.64	0.26	0.73
406	3092	0.010	0.076	2.68	0.043		0.137		1	2	919	0.225	3	2.04	0.51	1.24	0.44	2.13
420	7596	0.005	0.076	1.79	0.080	0.000	0.139	0.009	2	6	841	0.118	0					
428	3092	0.010	0.152	0.00	0.076		0.011		1	3	1159		2					